RSC Sustainability

ROYAL SOCIETY OF CHEMISTRY

PAPER

View Article Online
View Journal

Cite this: DOI: 10.1039/d5su00582e

Sustainable conductive ink for printing high performance wearable sensors

Cephas Amoah, [a] Ngoc Duc Trinh, [b] Chloé Bois[b] and W. G. Skene *[ac]

Advances in wearable sensors especially for health monitoring are breaking strides to meet the insatiable appetite for data that is demanded by the internet of things. This has been spurred on by fabricating sensors with conventional printing techniques. An underlying challenge is to improve the ecological impact of printing inks without sacrificing either their conductivity or sensor performance. To this end, we present a fully water soluble, self-doped conductive polymer (**pPDS**) ink formulated using environmentally benign water. The ink was optimized for conventional printing methods, flexography and screen printing, on a broad range of flexible substrates including fabrics, PET, and paper. The printed ink retained its intrinsic conductivity on the substrates and it enabled high performance relative humidity (RH) and temperature sensing. The response and recovery times of the sensors were 15 s and 26 s, respectively, at 22% and 75% RH, whereas the temperature sensor was independent of humidity at 40% and 80% RH with a −2.2% $°C^{-1}$ sensitivity. Unlike sensors based on conventional PEDOT:PSS and complex device architectures, the single-printed strip sensor offers a simple and straightforward alternative design for the potential non-invasive monitoring of respiration directly from printed textiles. The integration of sustainable conductive inks with direct-to-textile printing advances the field of wearable, passive health diagnostics, paving the way for scalable, environmentally responsible electronic sensing technologies.

Received 11th July 2025
Accepted 15th October 2025

DOI: 10.1039/d5su00582e

rsc.li/rscsus

Sustainability spotlight

This study presents a water-based conductive ink designed for printing wearable sensors on sustainable/recyclable substrates. The sensor features a minimalist design with humidity and temperature sensitivities comparable to complex architectures, significantly reducing material use and waste. The work advances sustainable wearable electronics manufacturing by eliminating toxic solvents for printing. The printed sensors can potentially enable non-invasive health monitoring from breathing. The sensors can ultimately be accessible to all owing to its simple design printed on readily available substrates. This innovation supports UN Sustainable Development Goals (SDG 3, SDG 9, SDG 12, and SDG 13) by promoting good health, responsible production, and sustainable industrial innovation. The approach provides scalable and environmentally responsible solutions for environmental sensing and potentially healthcare monitoring in the long term.

Introduction

Plastic electronics have garnered much attention owing to their fabrication advantages that surpass those of their metal and inorganic counterparts.[1–3] Their capacity to be printed using conventional large-scale techniques has further placed plastic electronics at the forefront for fabricating sustainable devices that are energy efficient.[4–6] The upscaled printing of the different components of plastic electronics on flexible substrates further opened new avenues for preparing energy efficient devices.[7,8] Indeed, sustainable devices have been fabricated on flexible substrates with conventional roll-to-roll printing methods such as flexography along with ink-jet and screen printing.[9–13]

Organic light emitting diodes (OLEDs), photovoltaics (OPVs), and thin-film transistors (TFTs) are among commonly printed devices.[14–18] Often overlooked devices that offer equally sustainable advantages include humidity and temperature sensors. These sensors play important roles in industrial, meteorological, and agricultural sectors as well as in human health especially for monitoring respiration and sweat detection.[19–22] These sensors leverage a unique layer of active material to provide high sensitivity along with both fast response and recovery times across a wide detection range.[23] Single layer sensors are advantageous for printing owing to their simple architecture, contrasting with other plastic electronics that are reliant on multilayer architectures.[24,25] Numerous materials have been employed toward achieving these goals

[a]Département de Chimie, Université de Montréal, Montréal, QC, Canada. E-mail: w.skene@umontreal.ca

[b]Institut des Communications Graphiques et de l'Imprimabilité, Montréal, QC, Canada

[c]Institut Courtois, Université de Montréal, Montréal, QC, Canada

including one-dimensional (1D) carbon, silicon, graphene, semiconductor nanoparticles, conducting polymers, and metal oxides among others.[26–36]

Conducting polymers such as polythiophenes are ideal for enabling humidity and temperature sensors because their intrinsic conductivity varies with these two stimuli. They also exhibit fast response and recovery times with subtle environmental changes.[37,38] Indeed, polythiophene sensors have high temperature sensitivities ($-0.77\%\ °C^{-1}$) while being independent of relative humidity (RH).[39] Flexible temperature sensors are also possible to construct with PEDOT:PSS composites using polydimethylsiloxane (PDMS) as an elastomer substrate without compromising the sensitivity ($0.63\%\ °C^{-1}$) and the fast response/recovery times (4.8/5.8 s).[40] The conductive polymer can also accurately detect variations in humidity between 18% and 77% RH that are common with human respiration.[41] The response rates (20–40 s) of such sensors also match the physiological rhythms, making them ideally suited for monitoring breathing.

Printing is the preferred method for fabricating sensors. This is in part because it is compatible with a wide range of substrates of different materials including fabrics and irregular shapes. Also, uniform layers of the sensor's active material components can be printed on a large scale.[3] This contrasts with spin- and spray-coating that are typically limited either to small areas of regular shape and smoothness or lead to rough layers of deposited materials, respectively. Both the printing method and the choice of substrate underpin the ink performance requirements.[42] Minimal requisites of the ink are surface wettability, moderate to high viscosity, and homogeneity of the active component in the ink. The ink viscosity can be adjusted by adding modifiers, such as polyethylene oxide (PEO). The additives are typically required in >0.5 wt% to improve the physical properties of the ink. This contrasts with conventional deposition methods that require a simple solution consisting uniquely of solvent and the given conductive polymer solute. Ink formulation is crucial because it underpins the performance of the sensor. However, formulating can be problematic with PEDOT:PSS because it is a dispersion. The requisite additives and modifiers can adversely affect the miscibility of the polymer. Ink modifiers can also reduce the polymer's intrinsic conductivity by both dedoping and increasing the insulating domains of PSS. These, in turn, affect the sensitivity and overall performance of the printed sensor.

Toward addressing these shortcomings, we pursued **pPDS** (Fig. 1) as an alternative polymer to PEDOT:PSS to formulate a conductive ink for printing sensors.[43–46] The advantages of this polymer are its homogeneity and solubility in water along with its self-doping. Therefore, it can be formulated into an ink with an environmentally benign solvent: water. Using sustainable solvents such as water is an important step toward improving the environmental fabrication footprint of sensors. Self-doping, on the other hand, would further increase the insensitivity of **pPDS** to additives and modifiers, resulting in consistent conductivity. As such, **pPDS** was formulated into a conductive ink for printing on polyethylene terephthalate (PET), paper, and fabric. These substrates were selected to demonstrate the universality of the sustainable ink for printing on various substrates by screen printing and flexography without the need for reformulating the ink for use with different media. Combined flexible RH and temperature sensors with high sensitivity and rapid-response rates are herein illustrated as tangible applications of the conductive ink with conventional printing methods. The performance of these sensors combined with their flexibility are ideally suited for monitoring physiological movements. Steps toward such true health monitoring are also demonstrated with a breath sensor printed from the sustainable ink.

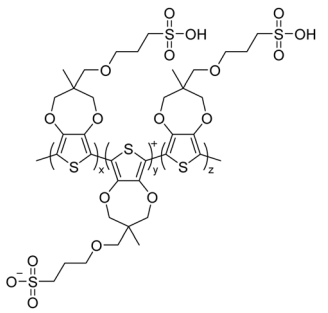

Fig. 1 Poly(propylenedioxythiophene sulfonate) (**pPDS**) conducting polymer used for formulating an aqueous conductive ink to print RH and temperature sensors *via* flexography and screen printing.

Materials and methods

Chemicals and reagents

All chemicals were used as received from commercial sources. Polyethylene oxide (PEO, 1.0 MDa) and neat sulphuric acid (H_2SO_4; 18 M) were obtained from Sigma-Aldrich. Dynol 960 and BYK-1709 were supplied by Evonik Industries and BYK-Chemie GmbH, Germany, respectively. **pPDS** was prepared as previously reported.[43,46] Commercially available polyethylene terephthalate (PET, thickness of 75 microns), fabric (polyester) and commercially available papers (Domtar Cougar and gloss coated papers) were used as substrates.

Printing techniques

Flexography printing was done with a Flexiproof 100-UV, RK Print Coat Instruments using different patterned printing plates. Two anilox volumes (15.0 and 6.48 BCM) were used with a printing speed of 20 m min^{-1} to print an area of 75 mm × 240 mm. Screen printing was done with an Ekra X1SL semi-automatic flatbed printing press with a maximum print area and substrate size of 304 mm × 304 mm and 460 mm × 460 mm, respectively. The squeegee was set at 70° and bilayering was possible after each drying cycle with positional cameras for overprinting.

Ink formulation

Conductive inks for flexography. The **pPDS** ink (30 mL) was prepared in water (1.0 wt%) with Dynol 960 (0.5 wt%). The conductive polymer was dissolved with vigorous stirring. PEO

(2.5 wt%) was added and the ink was stirred overnight. The ink was then blended with a speed mixer (DAC 330-100 PRO) at 1500 rpm for 3 min three times. The pH was adjusted with H_2SO_4 (2 M) to ensure the ink had pH < 4. The conductive homogeneous ink for printing was obtained by adding a defoamer (0.25 wt%, BYK-1709) after mixing with the speed mixer.

Conductive ink for screen printing. The screen printing ink was prepared (30 mL) with **pPDS** (2.0 wt%) and Dynol 960 (0.5 wt%) in water by vigorously stirring. PEO (5.0 wt% or 7.0 wt%) was added and the solution was stirred overnight. The viscous inks were homogenized with a speed mixer (1500 rpm) three times at 3 min each. The pH was adjusted with H_2SO_4 (2 M). Afterwards, the defoamer (0.25 wt%) was added followed by mixing with the speed mixer.

Characterization

Contact angles were measured (OCA LJ15 Dataphysics) to assess the wettability of the formulated conductive inks. The viscosity of the inks was also determined as a function of their shear rate with a rheometer (Anton Paar MCR 92). The sheet resistance of the ink printed on a given substrate was measured with an Ossila four-point probe and linear sweep voltammetry with a potentiostat (Biologic SP300). The printed design thickness was measured with a stylus profilometer (Bruker DektakXT). Scanning electron microscopy images were obtained after metalizing the samples with gold with an Agilent Phenom XL G2 benchtop scanning electron microscope (SEM) equipped with an energy-dispersive X-ray spectroscopy (EDS) detector.

Sensor fabrication

Sensors (2.0 × 2.0 cm) were prepared by printing the ink in a block pattern on the fabric substrate. Conductive copper tape was fixed to the opposite ends of the printed strip as electrical leads. These were connected to a potentiostat with alligator clips for measuring the resistance by linear sweep voltammetry (0–2.0 V). A hermetically sealed testing chamber (Binder MKF-56) was used to control both the temperature and relative humidity. For temperature sensing, the relative humidity of the chamber was maintained at either 40% RH and 80% RH and the relative resistance was measured as the temperature varied between 10 °C and 60 °C. The chamber was further open to ambient conditions to measure the true relative humidity under such conditions, *ca.* 80% RH. The temperature coefficient ratio (TCR), being the relative measured resistance as a function of temperature change, was graphically determined. The sensors were measured at a constant temperature of 20 °C between 20% and 80% RH for humidity sensing. The response time of the sensor was measured at 22% and 75% RH and this was taken as the time required to reach the TCR for the given RH.

Results and discussion

Ink formulation

The conductive **pPDS** ink was formulated by leveraging the well-established conventional CMYK ink formulation process. Also, knowledge of the effect of various additives and modifiers on the ink properties was also exploited for optimizing the conductive ink to meet the requirements for printing with different techniques. Key requirements the ink must satisfy for its use in printing are wettability, viscosity, shelf life (stability), drying properties and antifoaming. The latter is quintessential for aqueous inks. Using environmentally benign water as the solvent for the homogeneous **pPDS** ink has the advantages of a simplistic formulation for improving the overall sustainability of the ink compared to conventional PEDOT:PSS.

A conductive ink was formulated mainly by blending the water-soluble conducting polymer (**pPDS**) with polyethylene oxide (PEO) as a resin in water (Fig. 2A). PEO was selected because it is compatible with formulating the ink in water. Its principal role is to increase the viscosity by hydrogen bonding both with itself and water. The viscosity can, therefore, be adjusted to meet the requirements of a given printing method while keeping the amount of conductive polymer fixed. Viscosity is another property that governs the printability of the ink and it is printing method specific. An ink with low viscosity will uncontrollably cover the substrate, resulting in poor image fidelity. In contrast, an overly viscous ink cannot be coated and no ink will be transferred to the surface. Specifically, screen printing requires a viscous ink. This contrasts with flexographic printing that requires less viscous inks. The viscosity of the ink was quantified by rheology measurements with a shear rate of *ca.* 1000 s^{-1} being ideal for flexography.[47] This printing method involves inks being applied to an anilox cylinder for subsequent transfer to the flexographic printing plate. The ink is then transferred from the plate to the substrate (Fig. 2B).[48] This contrasts with screen printing that requires the ink to be more viscous, *ca.* 0.05–5 Pa s, for pressing through an opened mesh with the mesh producing the given image (Fig. 2C).

The viscosity requisites for the selected printing methods could readily be adjusted by varying the PEO concentration. However, increasing the amount of PEO reduced the electronic conductivity of the ink as PEO is an insulator similar to PSS. The concentration of **pPDS** was subsequently increased to 2 wt% to account for the insulating effect of the viscosity modifier. The viscosity of the ink at different shear rates was subsequently evaluated. The ideal formulations that met the 1000 s^{-1} viscosity threshold for flexographic and screen printing were 2.5 and 7.0 wt% PEO, respectively (Fig. 3).

Surfactants and defoaming agents were also added to the ink to further meet the printing requisites of the different substrates and the printing methods. The surfactant reduces the surface tension between the ink and the substrate when printing. The wettability of the ink on the substrate results in uniform coverage (*vide infra*), whereas the defoamer ensures the ink remains a liquid and it suppresses unwanted air bubbles that otherwise form when the ink is rapidly applied to the surface. This is important given foaming is notorious for aqueous inks, preventing uniform application of the ink on the surface. Foaming ultimately leads to a loss in both resolution and fidelity of the print. While these critical agents served important roles in the ink, they altered the pH of the conductive ink. This was problematic because the conductivity of **pPDS** is

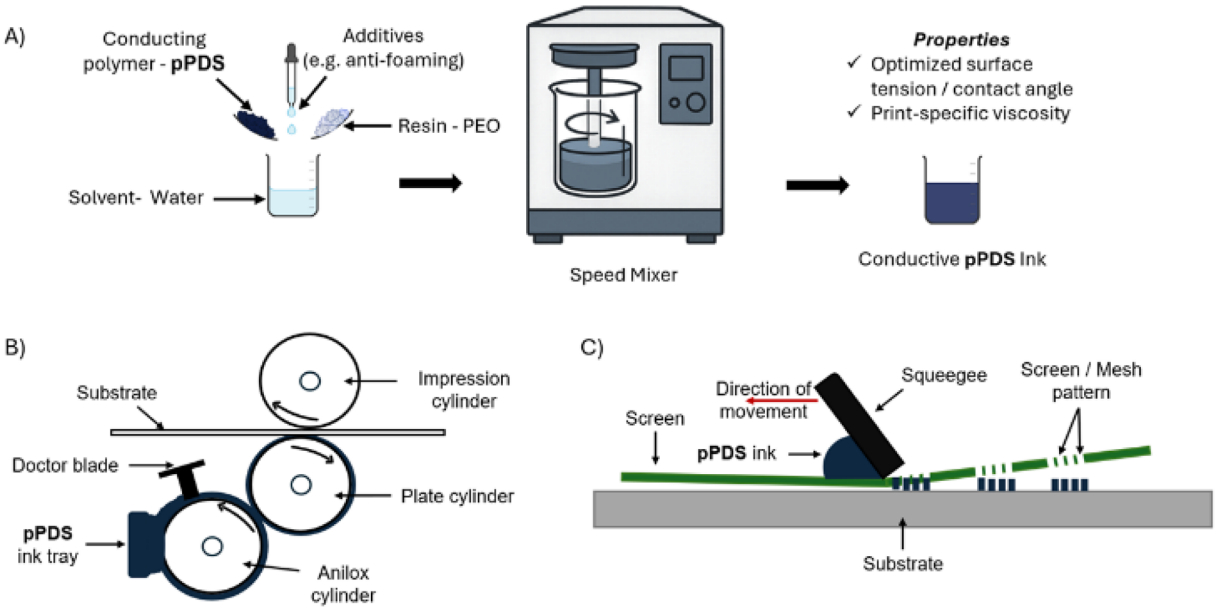

Fig. 2 Overview of ink formulation and printing techniques used to prepare patterned conductive substrates. Schematic representation of the **pPDS** conductive ink formulation (A), flexographic printing (B), and screen printing (C).

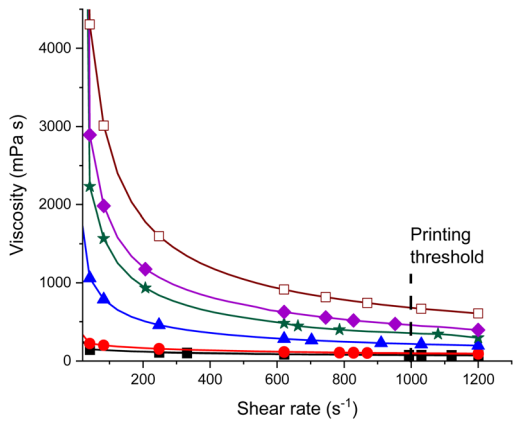

Fig. 3 Viscosity as a function of shear rate for different ink formulations of **pPDS** with varying wt% of PEO: 2 (black), 2.5 (red), 3 (blue), 4 (green), 5 (purple), and 7 wt% (wine).

contingent on pH, with desired high conductivity at pH < 4.[43] The pH of the ink was adjusted with mineral acid for the optimal conductivity of **pPDS**.

The surface adhesion of the ink to the given substrate further underpins the printability of the ink. Indeed, the ink must neither overwet the surface nor pearl when deposited, ensuring a uniform coverage of the ink on the surface along with a fidelity of the printed image. This critical parameter is tracked by conventional water contact angle measurements. The wettability of the ink is contingent on the surface. Given the ink is hydrophilic, the best wettability is expected with hydrophilic surfaces arising from either intrinsic polar functional groups or polar coatings on the substrate. In contrast, poor wettability is expected with hydrophobic surfaces or apolar coatings. The ink wettability of the surface was measured with inks that were formulated both with and without a surfactant (Fig. S1). The water contact angle of **pPDS** without the surfactant was identical to neat water as expected. The measured angles were 60°–77° contingent on the substrate with desired values being as close to 30° as possible. The contact angles were similar to reported values for 60°–82°.[49] Lowering the surface tension and enhancing the wettability of the ink was possible by adding a surfactant to the ink. Surfactant addition did lower the contact angle to 30°–40°.

Flexography and screen printing of conductive inks

Flexography and screen printing are among the most widely used techniques for printing conductive inks on substrates. These are owing to the ink requirements that can be met with conductive materials. Of importance, conductive materials such as conjugated polymers are soluble/miscible in solvents that can be used to coat various substrates. Conductive inks have been readily formulated by relying on well-established formulation of their conventional ink counterparts. The substrates for these printing methods are also compatible for the large-scale preparation of plastic electronics such as ITO coated PET. Flexography and screen printing were chosen to validate that the ink could indeed be printed with both high image fidelity and fine resolution for ultimately printing flexible electronics. The two conventional printing methods were chosen to evaluate the versatility of the inks because of their known contrasting print resolutions along with the preferred methods for large-scale printing.

Different designs were prepared with varying features, resolution, and details to validate the conductive ink was compatible with both flexography and screen printing without loss of image resolution and fidelity (Fig. 4, S2, and S3). While the print

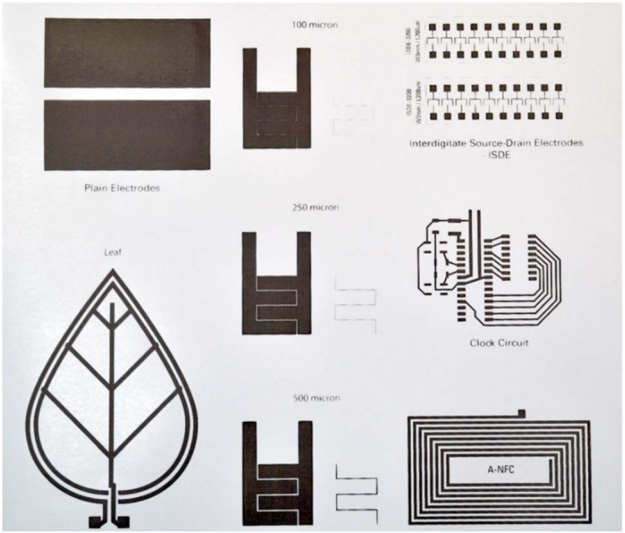

Fig. 4 Photograph of various designs with different resolutions printed with **pPDS** ink on paper. Dimensions of the paper printed: 304 mm × 304 mm.

resolution is contingent on the printing technique, both the flow and wettability of the ink affected the print resolution. Resolution upwards of 75 and 150 microns could be obtained by printing with **pPDS** *via* flexography and screen printing, respectively. High fidelity and resolution of the designs were maintained when printing **pPDS** on PET, paper, and fabric with single passes. The same ink formulation could be used for the various substrates. This confirms the universality of the ink for multi-substrate printing with the resolution of the image dictated by the intrinsic resolution of the printing method.

Printing multiple layers of the designs was also tested. This was to ensure the fidelity of the design. Multi-layer printing has the advantage of increasing the conductivity of the printed ink by depositing more material on the surface. Printing consecutive layers of the given designs on both paper and fabric was done by screen printing. Theses substrates were chosen because of their differences in ink absorption/adsorption. For example, the ink was absorbed immediately on paper once it was printed. Hence printing subsequent layers could be done without a drying cycle. The quality of the prints was unchanged when printing multiple layers. In contrast, the ink had to be dried between each print on PET. This required repositioning the image after each annealing step. The fidelity of the design was limited by the alignment of the design with the previously printed image.

The conductivity of the prints on the various substrates was measured with a four-point probe (Table 1). The conductivity of the flexographic print was 100 times lower than for screen printing. This is owing to the reduced amount of ink that is transferred to the substrate by flexography from the anilox cylinder (Table 1 and Fig. 2B). This contrasts with the screen printed designs that were thicker with more conductive ink printed on the surface. Designs printed on paper had lower conductivities relative to prints on PET. The decreased conductivity was from dedoping of the polymer by the paper (*vide infra*). The conversion of conductive **pPDS** to its nonconductive semi-conductor state when printing on paper was confirmed by the polymer's color change.[43]

Two layers of the given designs were printed by screen printing toward achieving the maximum conductivity of the printed ink. For example, the resistance decreased tenfold from the first layer to the second layer. The designs printed on the fabric were thicker at *ca.* 8 μm while the prints on paper were *ca.* 5 μm, and those on PET were *ca.* 2 μm (Table 1). The PET prints were thinner compared to prints on the other substrates even after printing a second layer. This was in part owing to the required drying step between printing of the subsequent layer. In contrast to PET, paper is porous and the ink was readily absorbed. Absorption removes the ink from the surface, lowering the effective amount of ink on the surface. This, in turn, reduced the conductivity of the prints. In contrast, fabric had excellent ink retention, giving rise to the thickest prints among the substrates. This, in turn, gave prints with the highest conductivity.

SEM micrographs of the prints on the various substrates were taken to gain insight into the surface coverage of the ink at the micron level. To better frame these results, both the native and the printed surfaces were imaged. The ink on PET was a contracted and non-contiguous film. Shrinkage of the ink was from the required drying step after printing the given layer (Fig. 5B *vs.* Fig. 5A). The ink printed on paper was contiguous and it covered the entire surface (Fig. 5D). The ink also coated the entire fabric and it adhered to the substrate (Fig. 5F). This was based on the difference in tint between the uncoated and coated images. The images also showed the ink pooled into islands. This was from ink absorption, resulting in different surface concentrations and subsequently different rates of solvent evaporation. The qualitative differences between the native (Fig. 5A, C and E) and the printed surfaces confirm the conductive ink is transferred to the substrate. This was further confirmed by the visibly detectable blue hue of the print that is characteristic of the conductive **pPDS**.

Energy-dispersive X-ray (EDX) measurements were also made on the SEM micrographs. These were to further confirm that the ink coated the surface. This was done by detecting the characteristic atomic composition of the polymer: sulfur. Indeed, sulfur was detected uniquely on the printed substrates and not in the native surfaces (Fig. S4–S6). Calcium oxides were further detected on paper by the EDX measurements on the surface. These render the surface alkaline and alter the intrinsic conductivity of ink upon printing (*vide supra*). This was corroborated by the visible purple hue of the prints on paper, which is associated with the dedoped polymer.[43] This is further supported by the EDX measurements that confirmed the presence of **pPDS** on the printed surfaces.

Fabric printed sensor

A sensor was fabricated by printing the ink directly on a fabric. The pattern consisted of a 2 cm × 2 cm solid strip. The sensor was completed by connecting copper lead electrodes for

Table 1 Sheet resistance and thickness measurement of the printed conductive ink on various substrates

	Flexography		Screen printing	
Substrate[a]	Anilox volume[b] (BCM)	Resistance[c] (MΩ sq^{-1})	Thickness[d] (μm)	Resistance[c] (kΩ sq^{-1})
PET	6.5	0.5–30	2.2 ± 0.1	113–850
Paper	15.0	>100	4.95 ± 0.08	>100 000
Fabric	—	—[e]	8.1 ± 0.2	12–143

[a] Fabric: polyester with intertwined yarns. [b] BCM: billion cubic microns. [c] Average resistance measured across the substrate. [d] Thickness of the deposited ink. [e] Substrate unsuitable for flexography printing.

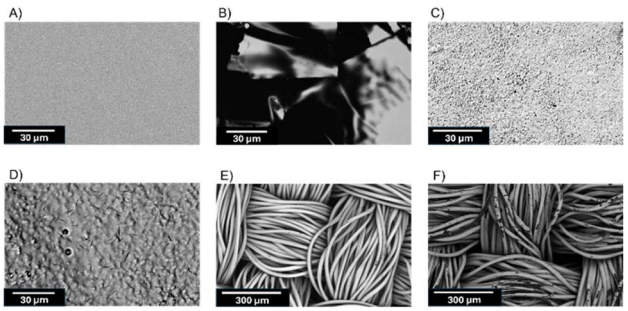

Fig. 5 SEM micrographs of **pPDS** ink printed on different substrates by screen printing: PET before (A) and after printing (B); paper before (C) and after printing (D); and fabric before (E) and after printing (F).

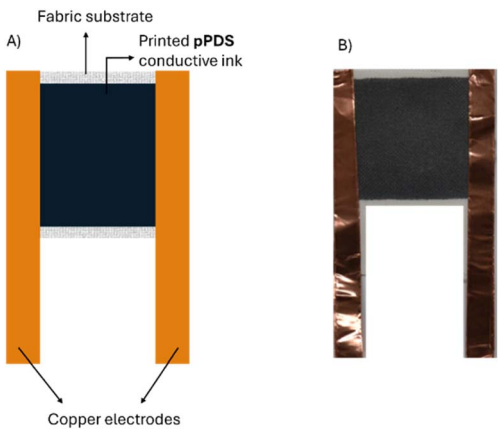

Fig. 6 (A) Representative diagram (2 cm × 2 cm) of the combined temperature and relative humidity sensor of **pPDS** printed on fabric (left). (B) Photograph of the operating fabric sensor printed on fabric (right).

subsequent attachment to a resistance meter (Fig. 6). Fabric was the choice substrate for printing because of **pPDS**'s higher conductivity when printed on this substrate. Moreover, the fabric is supple and flexible and it ultimately can be used as a wearable sensor. Printing directly on fabric provides the possibility of integrating sensors directly into clothing for real-time sensing of various stimuli. Temperature and humidity sensing were evaluated to illustrate the sensing capacity of the conductive print.

The operating principle of resistive sensors is their transduction of stimuli into measurable resistance. Temperature and relative humidity were the selected stimuli to measure. It is a common practice to quantify the stimuli of a resistive transducer according to the relative resistance ratio.[50,51] This is the difference between the resistance of a given stimulus and the resting resistance over the resistance in the resting state. Temperatures ranging from 10° to 60 °C were measured to determine the sensing capacity of the device to this stimulus (Fig. 7A). The temperature was adjusted in 10 °C intervals while the RH was regulated in a climate chamber. The effect of the

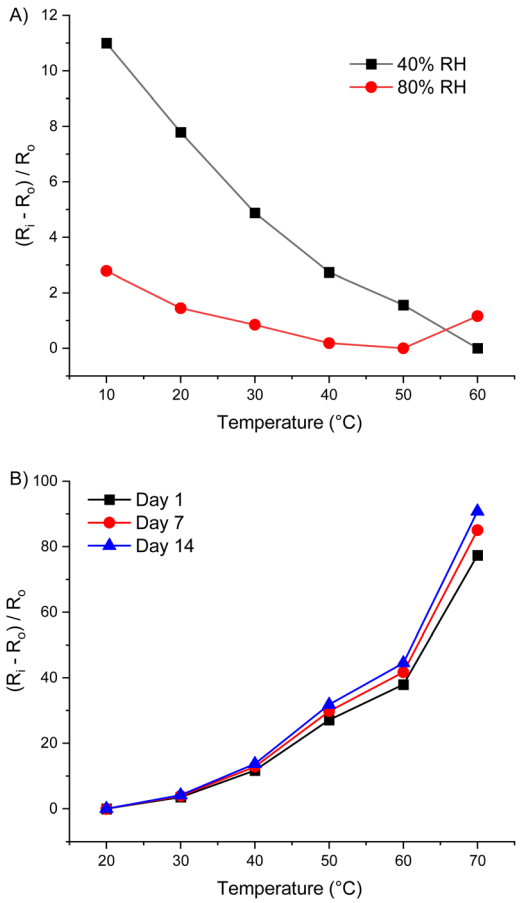

Fig. 7 **pPDS** sensor printed on fabric for measuring temperature changes at 40% and 80% RH according to differential resistance (A) and consistent temperature measurements over several days at ambient RH (B).

relative humidity on the temperature sensor was also evaluated at 40% and 80%. These RH extremes were chosen because they represent standard room conditions on the low end of the scale and typical outdoor seasonal conditions on the opposite scale. The resistance ratio of the sensor could be used to track the change in temperature. Indeed, the resistance ratio decreased with increasing temperature at fixed RH as per Fig. 7A. The resistance ratio was also contingent on the relative humidity, with significant differences between the RH extremes for a given temperature. The observed temperature induced resistance change was a direct result of temperature variations since the humidity was constant. The temperature sensitivity arises from enhanced transport of the charge carriers and inter- and intra-carrier hopping and tunneling by extended planarization of the conjugated framework with increasing temperature.[39,52,53] A second environment was created. Here, the humidity changes were uncontrolled and they were dependent on the temperature changes between 20 °C and 70 °C. The same response was observed with the sensor for both the change in temperature and RH over several days (Fig. 7B). The reproducibility of the sensor was confirmed by the consistent resistance ratios that were repeatedly measured over 14 days. It is worth noting that RH is inversely related to temperature. As such, the detection mechanism of the sensor at temperature extremes is different. On one hand, the water absorbed by the sensor at low temperatures/high RH promotes charge transfer through the thin layer of water adsorbed on the surface. This enhances the conductivity, leading to lower resistance ratios. On the other hand, changes in conductivity at high temperatures/low RH are uniquely from the temperature coefficient of resistance of the polymer. Charge transport is less effective with this mechanism, resulting in lower relative resistance and high resistance ratios. These different conductive mechanisms are the origin of the behavior in Fig. 7B.

The sensitivity of the sensor toward temperature, and hence, its capacity to accurately measure temperature can be derived by its temperature coefficient. This refers to the change in resistance per change in temperature. The temperature coefficient of the fabric sensor was moderate: $-2.2\%\ °C^{-1}$ for the 20–60 °C range. Highly sensitive detectors have temperature coefficients in the -0.77 to $0.63\%\ °C^{-1}$ range.[39,40] These sensitive sensors are reliant on complex device architectures along with composite conductive materials. Bearing this in mind, the benefit of the **pPDS** sensor is its simplistic architecture that consists of a single printed strip from a unique water-soluble component with reasonable sensitivity.

Given the different responses of the sensor at extreme RH, the sensor's capacity to detect changes in relative humidity was also assessed. This was done by varying the relative humidity in a controlled environment between 20% and 80% RH at a constant temperature. The resistance ratio indeed varied with RH (Fig. 8A) with the conductivity of the **pPDS** ink increasing concomitantly with RH. This is a result of water absorption by the ink that favors the transfer of charge carriers by increasing the percolation pathways.

The cloth sensor was subjected to alternating RH to confirm its consistent and reproducible change in resistance ratio with RH. For this, the sensor was placed in an environment of 22% RH. After the resistance ratio equilibrated, the sensor was transferred to a 75% RH environment and equilibrated once again. Switching between the two environments of different RH was repeated over multiple cycles (Fig. 8B). Of importance is the consistent response of the sensor to both RH environments. This confirms that the resistance can be used as a reliable parameter to detect relative humidity. It further confirms that a calibration curve can be reliably used to determine the absolute humidity levels from the resistance ratio contingent on temperature.

The response rate of the printed sensor toward changes in humidity can be derived from cycles of switching between a given set of humidities. The response time of the sensor toward increased humidity was 15.4 s. The time required to recover the original resistance ratio when returning to lower humidity was nearly twice as slow (26.5 s; Fig. 8C). The ink is nonetheless responsive to changes in humidity, recovering the original resistance ratio (*vide supra*). The response rates of humidity sensors using PEDOT:PSS as the responsive transducer are found in Table 2 to frame the responsiveness of the **pPDS** ink. While many humidity sensors are known, PEDOT:PSS sensors were selected for comparison given the structural similarity of this conductive polymer and responsive mechanism to **pPDS**. The response and recovery time of the **pPDS** sensor was on par with its PEDOT:PSS counterparts. The printed sensor was further sensitive across the range of studied humidities. It is worthwhile noting that the benchmarked sensors were composites of either graphene[54] or inorganics to ensure both their response rates and sensitivity. They were also fabricated using less than straightforward processes while relying on rigid substrates and complex patterns. Bearing these in mind, the **pPDS** printed sensor outperformed these sensors when taking into account the ink can be printed on wearable substrates using common printing methods. The printed **pPDS** sensor further excels in its design simplicity, consisting of a simple solid pattern: a unique strip of ink.

Applications of humidity sensing

Humidity sensing can be extended to include tangible uses other than ambient relative humidity. Of interest is leveraging humidity tracking in the biomedical context. For example, monitoring human breathing has emerged as a non-invasive tool for both detecting and diagnosing diseases and disorders. These include liver, cardiac, pulmonary, and early-stage lung cancer diagnoses.[41,60–62] These can be monitored through a disorder in the patient's humidity patterns that are monitored during breathing. Toward such monitoring, the **pPDS** sensor was applied to track human respiration. This was to further illustrate the true sensing application of the simplistic sensor. The sensor was used to monitor human respiration as a proof-of-concept. For this, the sensor tracked human breathing through the mouth and normal breath patterns. The sensor monitored the humidity upon exhaling with the amount of moisture detected correlating with the breathing depth. Consistent resistance ratios were indeed measured when

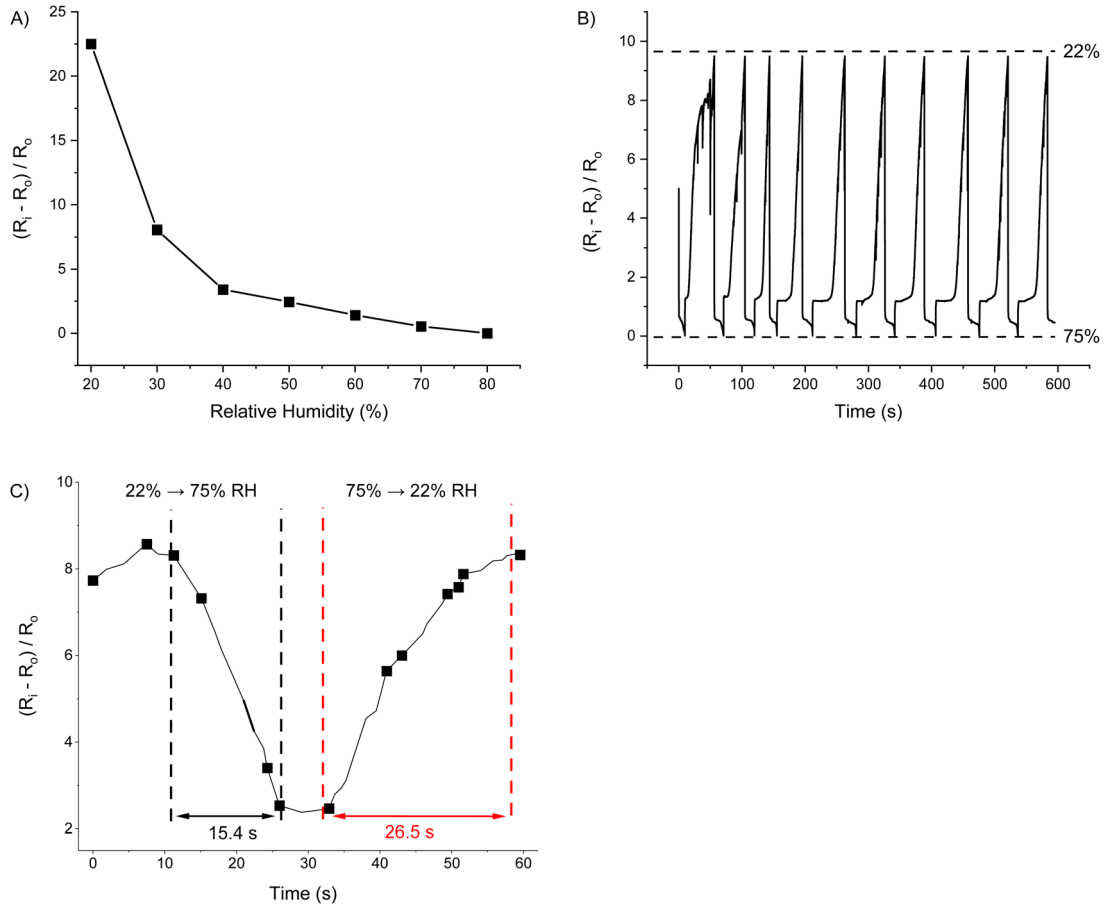

Fig. 8 Humidity sensing according to the change in the resistance ratio of **pPDS** printed on fabric. (A) Relative humidity sensing at 20 °C. (B) Recovery and response times of the sensor of multiple cycles of switching between 22% (lower) and 75% (upper) RH. (C) Recovery (red) and response (black) times of switching between 22% and 75% RH.

breathing under normal conditions without stress (Fig. 9A). The signal amplitude was consistent with breathing both *via* the mouth and the nose. This aside, the humidity responsive profiles were different for nasal and oral breathing. Nasal breathing gave sharper resistance ratios as a function of time compared to breathing through the mouth. This is owing to exposure differences of the sensor to the moist air. On one hand, exhaling through the mouth produces an abrupt flow of air in a short period. This contrasts with nasal breathing that delivers a continuous flow of air over a longer period of time. In both cases, the total amounts of air and moisture that are produced are the same, resulting in near-identical signal amplitude differences. Yet, the rate of producing the moist air is evidenced by the signal's width: broad for continuous streams such as yawning (Fig. 9B) and narrow for breathing *via* the mouth. This proof-of-concept validates the sensor's use in

Table 2 Comparative relative humidity sensing of various sensors

Material[a]	Fabrication method[b]	Sensitivity range (RH%)	Response/recovery time (s)	Ref.
pPDS/PEO	Screen printing	20–80[c]	15/26	This work
GO/PEDOT:PSS	Laser direct writing	11–97	5/16.5	55
Sn_2O	CVD	5–85	120/60	56
PEDOT:PVMA	Inkjet printing	11–98	—[d]	57
PEDOT:PSS/RGO	Inkjet printing	0–98	39/57	58
PEDOT:PSS/GO	CVD	12–97	31/72	20
PEDOT:PSS/PEO	Drop casting	6–92	11–20/20–28	41
MoS_2/PEDOT:PSS	Thin layer deposition	0–80	0.5/0.8	59

[a] RGO: reduced graphene oxide; PVMA: 7-(4-vinylbenzyloxyl)-4-methylcoumarin (VM) and maleic anhydride (MA) copolymer. [b] CVD: chemical vapor deposition. [c] Instrumental limitation prevented measuring outside the reported RH% range. [d] Not determined.

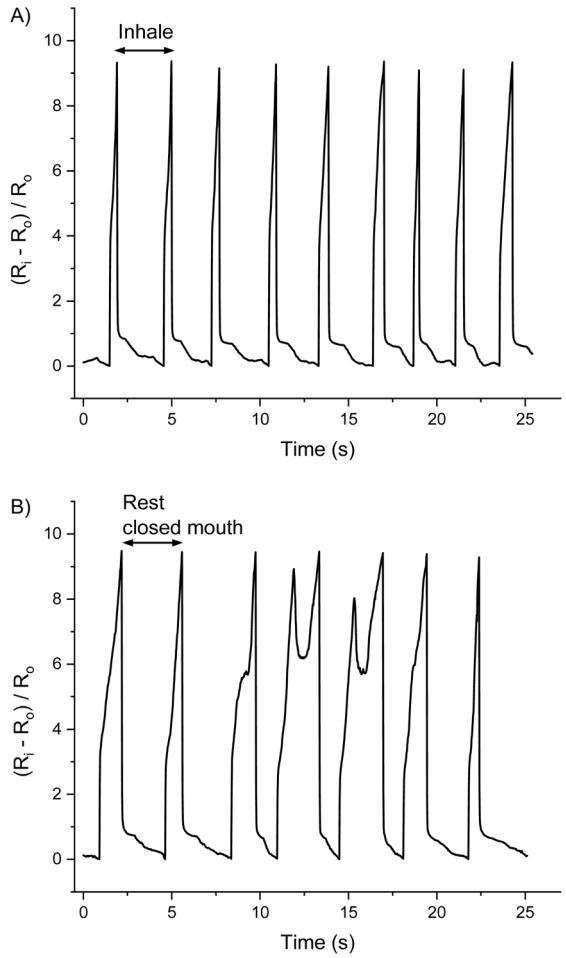

Fig. 9 Printed **pPDS** humidity sensor on fabric for monitoring human respiration (A) and yawning (B).

monitoring physiological outcomes. Ultimately, the straightforward fabrication of the sensor can potentially be used for detecting apnea along with signaling labored breathing for preemptively detecting respiratory distress and for predicting underlying health conditions. Integrating biosensors into the conductive ink provides the possibility of non-invasive and selective detection of given ailments by resistive transduction.

Conclusions

In summary, a conductive ink using environmentally benign water was formulated. The ink could be printed on various flexible substrates including recyclable materials by both screen printing and flexography for preparing combined temperature and humidity sensors. The prints had high fidelities with the designs, and the resolution was contingent on the printing technique. The conductivity of the printed ink was also dependent on the substrate. The sensitivity and response times of the combined printed humidity and temperature sensors surpassed the performance of sensors prepared from PEDOT:PSS when considering the simplicity of the sensor design. The sensors could further be used in tangible physiological applications by monitoring human respiratory patterns. Printing on fabrics serves as a proof-of-concept that sensors can seamlessly be integrated into clothing for wearable electronics, whereas printing on paper provides new possibilities for recycling sensors after their use and further improving their overall environmental footprint. Eventually modifying the conjugated polymer by integrating biosensors further expands the use of sensors by exploiting physiological movements for the non-invasive detection and diagnosis of respiratory-related diseases.

Author contributions

Conceptualization, formal analysis, methodology, and writing: CA and WGS; supervision: WGS, NDT, and CB; validation: CA, WGS, NDT, and CB; the manuscript was written through contributions of all authors. All authors have given approval to the final version of the manuscript.

Conflicts of interest

There are no conflicts to declare.

Data availability

All data from the study are included in this published article and its corresponding supplementary information (SI). Supplementary information: water contact photographs, flexography designs on PET and paper, and energy dispersive X-ray spectra of **pPDS** on PET, paper, and fabric. See DOI: **https://doi.org/10.1039/d5su00582e**.

Acknowledgements

The Natural Science and Engineering Research Council Canada (NSERC) and the Canada Foundation for Innovation are thanked for funding and equipment, respectively, that supported this collaborative research. C. A. also thanks the Fonds de Recherche Quebecois Science and Nature (FRQNT) for a graduate scholarship. C. A. also appreciates the assistance of the R&D department within the Institut des Communications Graphiques et de l'Imprimabilité (ICI) led by M. Torres.

Notes and references

1 T. B. Singh and N. S. Sariciftci, *Annu. Rev. Mater. Res.*, 2006, **36**, 199–230.
2 G.-J. N. Wang, A. Gasperini and Z. Bao, *Adv. Electron. Mater.*, 2018, **4**, 1700429.
3 C. Amoah, U. Mahmood and W. G. Skene, *Adv. Mater. Technol.*, 2025, 2401600.
4 G. Blanchet and J. Rogers, *J. Imaging Sci. Technol.*, 2003, **47**, 296–303.
5 J. Wiklund, A. Karakoç, T. Palko, H. Yigitler, K. Ruttik, R. Jäntti and J. Paltakari, *J. Manuf. Mater. Process.*, 2021, **5**, 89.

6 Y. Chen, Z. Liu, Z. Wang, Y. Yi, C. Yan, W. Xu, F. Zhou, Y. Gao, Q. Zhou, C. Zhang and H. Deng, *Adv. Sci.*, 2024, **11**, 1–13.
7 J. A. Rogers and Z. Bao, *J. Polym. Sci., Part A: Polym. Chem.*, 2002, **40**, 3327–3334.
8 J. M. J. Fréchet, *Prog. Polym. Sci.*, 2005, **30**, 844–857.
9 C. Kim, K. An, M. Kang, P. Won, J. J. Park, K. H. Cho, S. H. Ko, B. K. Ju and K. T. Kang, *Sci. Rep.*, 2022, **12**, 1–8.
10 A. Morrin, O. Ngamna, E. O'Malley, N. Kent, S. E. Moulton, G. G. Wallace, M. R. Smyth and A. J. Killard, *Electrochim. Acta*, 2008, **53**, 5092–5099.
11 T. Cosnahan, A. A. R. Watt and H. E. Assender, *Mater. Today: Proc.*, 2018, **5**, 16051–16057.
12 S. Tong, J. Yuan, C. Zhang, C. Wang, B. Liu, J. Shen, H. Xia, Y. Zou, H. Xie, J. Sun, S. Xiao, J. He, Y. Gao and J. Yang, *npj Flexible Electron.*, 2018, **2**, 1–8.
13 J. Kim, P. Jepiti, M. Lee, E. Park, R. Phon and S. Lim, *Mater. Des.*, 2024, **247**, 113451.
14 S. Chung, K. Cho and T. Lee, *Adv. Sci.*, 2019, **6**, 1801445.
15 A. Hübler, B. Trnovec, T. Zillger, M. Ali, N. Wetzold, M. Mingebach, A. Wagenpfahl, C. Deibel and V. Dyakonov, *Adv. Energy Mater.*, 2011, **1**, 1018–1022.
16 J. Hast, M. Tuomikoski, R. Suhonen, K.-L. Väisänen, M. Välimäki, T. Maaninen, P. Apilo, A. Alastalo and A. Maanineny, *SID Symp. Dig. Tech. Pap.*, 2013, **44**, 192–195.
17 X. Y. Zeng, Y. Q. Tang, X. Y. Cai, J. X. Tang and Y. Q. Li, *Mater. Chem. Front.*, 2023, **7**, 1166–1196.
18 K. Matura, C. Putz, S. Hradilova, K. Polakova, M. Irimia-Vladu, M. Okajima, T. Kaneko, M. Kaltenbrunner, N. S. Sariciftci and S. Tekoglu, *npj Flexible Electron.*, 2025, **9**, 56.
19 J. Liu, M. Agarwal, K. Varahramyan, E. S. Berney IV and W. D. Hodo, *Sens. Actuators, B*, 2008, **129**, 599–604.
20 Y. Pang, J. Jian, T. Tu, Z. Yang, J. Ling, Y. Li, X. Wang, Y. Qiao, H. Tian, Y. Yang and T. L. Ren, *Biosens. Bioelectron.*, 2018, **116**, 123–129.
21 W. Shi, Z. Wang, H. Song, Y. Chang, W. Hou, Y. Li and G. Han, *ACS Appl. Mater. Interfaces*, 2022, **14**, 35114–35125.
22 M. Ikram, S. Ameer, F. Kulsoom, M. Sher, A. Ahmad, A. Zahid and Y. Chang, *Comput. Electron. Agric.*, 2024, **226**, 109449.
23 H. Bi, K. Yin, X. Xie, J. Ji, S. Wan, L. Sun, M. Terrones and M. S. Dresselhaus, *Sci. Rep.*, 2013, **3**, 1–7.
24 M. Tekcin, E. Sayar, M. K. Yalcin and S. K. Bahadir, *Electronics*, 2022, **11**, 1025.
25 C. Beaumont, R. Lapointe, P. Beaupré, C. Trudeau, N. Le Bouch and M. Leclerc, *Flexible Printed Electron.*, 2022, **7**, 044006.
26 A. Beniwal, D. A. John and R. Dahiya, *IEEE Sens. Lett.*, 2023, **7**, 1–4.
27 X. Chen, J. Zhang, Z. Wang, Q. Yan and S. Hui, *Sens. Actuators, B*, 2011, **156**, 631–636.
28 Y. Zilberman, R. Ionescu, X. Feng, K. Müllen and H. Haick, *ACS Nano*, 2011, **5**, 6743–6753.
29 Q. Kuang, C. Lao, L. W. Zhong, Z. Xie and L. Zheng, *J. Am. Chem. Soc.*, 2007, **129**, 6070–6071.
30 S. Borini, R. White, D. Wei, M. Astley, S. Haque, E. Spigone, N. Harris, J. Kivioja and T. Ryhänen, *ACS Nano*, 2013, **7**, 11166–11173.
31 D. Lei, Q. Zhang, N. Liu, T. Su, L. Wang, Z. Ren, Z. Zhang, J. Su and Y. Gao, *Adv. Funct. Mater.*, 2022, **32**, 1–12.
32 J. Yang, D. Wei, L. Tang, X. Song, W. Luo, J. Chu, T. Gao, H. Shi and C. Du, *RSC Adv.*, 2015, **5**, 25609–25615.
33 S. N. Aidit, F. A. M. Rezali, N. H. M. Nor, N. Yusoff, L.-Y. Ma, S. F. W. M. Hatta and N. Soin, *Flexible Printed Electron.*, 2023, **8**, 025008.
34 W. A. Daoud, J. H. Xin and Y. S. Szeto, *Sens. Actuators, B*, 2005, **109**, 329–333.
35 W. Liu, R. Xie, J. Zhu, J. Wu, J. Hui, X. Zheng, F. Huo and D. Fan, *npj Flexible Electron.*, 2022, **6**, 1–10.
36 J. Zhong, Z. Xia, C. Zhang, B. Li, X. Liu, Y.-B. Cheng and J. Tang, *Chem. Mater.*, 2014, **26**, 3573–3578.
37 M. A. Farea, H. Y. Mohammed, S. M. Shirsat, M.-L. Tsai, M. N. Murshed, M. E. El Sayed, S. Naji, A. Samir, R. M. Alsharabi and M. D. Shirsat, *Mater. Sci. Semicond. Process.*, 2023, **155**, 107255.
38 F. J. Romero, A. Rivadeneyra, M. Becherer, D. P. Morales and N. Rodríguez, *Micromachines*, 2020, **11**, 148.
39 Y. F. Wang, T. Sekine, Y. Takeda, K. Yokosawa, H. Matsui, D. Kumaki, T. Shiba, T. Nishikawa and S. Tokito, *Sci. Rep.*, 2020, **10**, 1–8.
40 Z. Zhu, Y. Su, J. Chen, J. Zhang, L. Liang, Z. Nie, W. Tang, Y. Liang and H. Li, *ACS Appl. Mater. Interfaces*, 2024, **16**, 56082–56094.
41 E. Assunção da Silva, C. Duc, N. Redon and J. L. Wojkiewicz, *Macromol. Mater. Eng.*, 2021, **306**, 1–10.
42 M. R. Repon, T. Islam, T. K. Paul, S. Jurkonienė, A. Haji, S. Shukhratov and G. F. I. Toki, *Environ. Sci. Pollut. Res.*, 2024, **31**, 47552–47583.
43 C. Amoah, J. F. Terán Morales, U. Mahmood and W. G. Skene, *ACS Appl. Electron. Mater.*, 2025, **7**, 1745–1755.
44 D. M. Welsh, A. Kumar, M. C. Morvant and J. R. Reynolds, *Synth. Met.*, 1999, **102**, 967–968.
45 L. Groenendaal, G. Zotti, P. H. Aubert, S. M. Waybright and J. R. Reynolds, *Adv. Mater.*, 2003, **15**, 855–879.
46 H. Yano, K. Kudo, K. Marumo and H. Okuzaki, *Sci. Adv.*, 2019, **5**, 1–10.
47 Z. Wang, R. Winslow, D. Madan, P. K. Wright, J. W. Evans, M. Keif and X. Rong, *J. Power Sources*, 2014, **268**, 246–254.
48 N. Hedayat, Y. Du and H. Ilkhani, *Renewable Sustainable Energy Rev.*, 2017, **77**, 1221–1239.
49 T. Homola, L. Y. L. Wu and M. Černák, *J. Adhes.*, 2014, **90**, 296–309.
50 Z. Gao, L. Kong, R. Jin, X. Liu, W. Hu and G. Gao, *J. Mater. Chem. C*, 2020, **8**, 11119–11127.
51 E. Verpoorten, G. Massaglia, C. F. Pirri and M. Quaglio, *Sensors*, 2021, **21**, 4110.
52 A. M. Nardes, M. Kemerink and R. A. J. Janssen, *Phys. Rev. B: Condens. Matter Mater. Phys.*, 2007, **76**, 085208.
53 E. Vitoratos, S. Sakkopoulos, E. Dalas, N. Paliatsas, D. Karageorgopoulos, F. Petraki, S. Kennou and S. Choulis, *Org. Electron.*, 2009, **10**, 61–66.
54 G. Hassan, M. Sajid and C. Choi, *Sci. Rep.*, 2019, **9**, 1–10.

55 Y. Song, R. Dan, L. Li, X. Xia, J. Zhao and R. Xu, *Sens. Actuators, A*, 2025, **387**, 116433.
56 Q. Kuang, C. Lao, Z. L. Wang, Z. Xie and L. Zheng, *J. Am. Chem. Soc.*, 2007, **129**, 6070–6071.
57 Y. Yuan, Y. Zhang, R. Liu, J. Liu, Z. Li and X. Liu, *RSC Adv.*, 2016, **6**, 47498–47508.
58 Y. Yuan, B. Peng, H. Chi, C. Li, R. Liu and X. Liu, *RSC Adv.*, 2016, **6**, 113298–113306.
59 G. U. Siddiqui, M. Sajid, J. Ali, S. W. Kim, Y. H. Doh and K. H. Choi, *Sens. Actuators, B*, 2018, **266**, 354–363.
60 S. T. Krishnan, J. P. Devadhasan and S. Kim, *Anal. Bioanal. Chem.*, 2017, **409**, 21–31.
61 J. Zhou, Z.-A. Huang, U. Kumar and D. D. Y. Chen, *Anal. Chim. Acta*, 2017, **996**, 1–9.
62 M. Peng, D. Lv, D. Xiong, W. Shen, W. Song and R. Tan, *J. Electron. Mater.*, 2019, **48**, 2373–2381.